Optics Letters

Octave-spanning coherent supercontinuum generation in a silicon nitride waveguide

Adrea R. Johnson,[1,*] Aline S. Mayer,[2] Alexander Klenner,[2] Kevin Luke,[3] Erin S. Lamb,[1] Michael R. E. Lamont,[1,3,4] Chaitanya Joshi,[1] Yoshitomo Okawachi,[1] Frank W. Wise,[1] Michal Lipson,[3,4] Ursula Keller,[2] and Alexander L. Gaeta[1,4]

[1]School of Applied and Engineering Physics, Cornell University, Ithaca, New York 14853, USA
[2]Department of Physics, Institute of Quantum Electronics, ETH Zurich, 8093 Zurich, Switzerland
[3]School of Electrical and Computer Engineering, Cornell University, Ithaca, New York 14853, USA
[4]Kavli Institute at Cornell for Nanoscale Science, Cornell University, Ithaca, New York 14853, USA
*Corresponding author: arj46@cornell.edu

Received 11 August 2015; accepted 9 September 2015; posted 1 October 2015 (Doc. ID 247575); published 30 October 2015

We demonstrate the generation of a supercontinuum spanning more than 1.4 octaves in a silicon nitride waveguide using sub-100-fs pulses at 1 μm generated by either a 53-MHz, diode-pumped ytterbium (Yb) fiber laser or a 1-GHz, Yb:$CaAlGdO_4$ (Yb:CALGO) laser. Our numerical simulations show that the broadband supercontinuum is fully coherent, and a spectral interference measurement is used to verify that the supercontinuum generated with the Yb:CALGO laser possesses a high degree of coherence over the majority of its spectral bandwidth. This coherent spectrum may be utilized for optical coherence tomography, spectroscopy, and frequency metrology.

OCIS codes: (320.6629) Supercontinuum generation; (190.4390) Nonlinear optics, integrated optics.

http://dx.doi.org/10.1364/OL.40.005117

Coherent supercontinuum generation (SCG) has been utilized as a phase-coherent broadband source for biological imaging and molecular detection techniques, such as optical coherence tomography [1] and coherent Raman [2] and anti-stokes Raman spectroscopy [3]. A phase-coherent optical spectrum is also critical for applications including pulse compression [4], frequency metrology [5–8], and wavelength division multiplexing [9]. Additionally, coherent supercontinuum (SC) with an octave-spanning bandwidth is highly desirable for the detection of the carrier envelope offset frequency (f_{ceo}) of a modelocked laser through a self-referencing scheme using f-$2f$ interferometry [5,6], enabling a fully stabilized frequency comb source. For some applications, such as dual-comb spectroscopy, where the resolution is determined by the comb spacing, the desired source repetition rate is determined by the sample that is characterized [10,11]. Thus a SC platform that can operate over a wide range of pulse energies and repetition rates is highly advantageous. Coherent SC for these applications may be generated in a fiber-based or chip-based platform. However, chip-based SCG offers the potential for cost-efficient, large-scale production and, more importantly, the potential for a completely integrated photonic SC source.

Current chip-based SCG platforms include silicon [12–16], amorphous silicon [17], silica [18], high-index-doped silica [19], silicon nitride [20–26], chalcogenide [27–30], and periodically poled lithium niobate waveguides [31]. Silicon-based waveguides in particular provide material compatibility with existing complementary metal-oxide-semiconductor (CMOS) fabrication technology that allows for wide-scale implementation of integrated chip-scale devices. Silicon nitride (Si_3N_4) is a CMOS-compatible material with a nonlinearity ($n_2 = 2.5 \times 10^{-15}$ $cm^2\,W^{-1}$) that is two times larger than that of high-index-doped silica and 10 times larger than that of silica [32]. This high nonlinearity coupled with the high-mode confinement allows for short waveguide lengths, which enables coherent SCG. The large band gap of Si_3N_4, as compared to either crystalline or amorphous silicon [32,33], allows for nonlinear interactions that are free from two-photon absorption at near-infrared wavelengths, making Si_3N_4 an ideal candidate for SCG at 1 μm. Previous demonstrations of SCG in Si_3N_4 with near-infrared [20–25] and mid-infrared [26] pump lasers have achieved octave-spanning bandwidths, but the coherence of the generated SC spectra has not been characterized.

Here we investigate the coherence of SC spectra spanning more than an octave generated in Si_3N_4 waveguides using sub-100-fs, 1 μm pulses from a 53-MHz diode-pumped ytterbium (Yb) fiber laser and a 1-GHz Yb:$CaAlGdO_4$ (Yb:CALGO) laser. For each laser source, we observe similar spectral features in the experimentally generated SC, and numerical simulations of the generated spectra show a high mutual coherence over the entire spectral bandwidth. Moreover, for both laser sources, a broadband SC is generated with low coupled pulse energies (~36 pJ in the waveguide). This low power requirement stems from the high mode confinement and high nonlinearity at 1 μm, which combine to give a high nonlinear coefficient ($\gamma \sim 3$ $W^{-1}\,m^{-1}$) that allows for SCG from these laser sources without additional amplification. In our experiments, we apply

a spectral coherence measurement in which the SC generated from a single input pulse is interfered with the spectrum generated from an adjacent pulse. From this measurement, we find that the generated SC is highly coherent over the majority of its bandwidth and is suitable for $f-2f$ interferometry.

We achieve coherent broadband SCG in a Si_3N_4 ridge waveguide through careful design of the dispersion. SCG at a specific pump wavelength is accomplished through modification of the waveguide cross section to tailor the appropriate contribution from the waveguide dispersion. Based on our 1-μm pump, the waveguide cross section is designed to achieve a broad region of anomalous group-velocity dispersion (GVD) about the pump wavelength. Figure 1 shows the simulated GVD for two waveguides with different widths. The region of anomalous GVD at the pump wavelength and the two zero-GVD points allow for coherent SCG when pumping with adequately short pulses through self-phase modulation and the emission of a dispersive wave on either side of the pump wavelength which serves to extend the coherent bandwidth of the generated SC [34, 35].

In our experiment, we first demonstrate SCG using a 53-MHz, dispersion-managed soliton fiber laser [36]. We use an 8-mm-long Si_3N_4 waveguide with a cross section of 690 × 950 nm (see Ref. [37] for fabrication details). The waveguide is pumped with 92-fs pulses and 437 pJ of pulse energy incident on the waveguide. The laser pulses have a center wavelength of 1030 nm and are assumed to have a Gaussian intensity profile. The polarization of the input pulses is adjusted to quasi-TE with a half-wave plate, and an aspheric objective is then used to couple the light into the chip with an 11-dB coupling loss, which is determined using an aspheric objective at the output of the waveguide. The coupling loss is not fundamental and may be improved in future designs through optimization of the inverted taper to promote coupling into the fundamental mode. We measure the propagation loss of the waveguide to be 0.7 dB/cm at 1550 nm. The output light is collected with a lensed fiber with a 3-dB coupling loss and sent to two different optical spectrum analyzers (OSAs). One OSA is used to cover the wavelength range from 350 to 1750 nm, and a second OSA is used to measure the wavelength range from 1200 to 2400 nm after spectral components below 1200 nm are filtered to prevent higher-order diffraction effects. Figure 2(a) shows the experimental SC spectrum generated with 35 pJ of pulse energy in the waveguide. The spectrum spans the wavelength range from 673 to 1944 nm, which corresponds to 1.5 octaves of bandwidth measured at −40 dB relative to the peak of the spectrum.

We theoretically investigate the coherence of the SC spectrum by performing numerical SCG simulations using the split-step Fourier method to solve the generalized nonlinear Schrödinger equation, including third-order nonlinearity, higher-order dispersion, and self-steepening. Raman effects are not included. To characterize the spectral coherence, the input pulses are seeded with quantum shot noise [38]. The simulated SC for an 8-mm-long waveguide with 92-fs pump pulses and 25.5 pJ of coupled pulse energy is shown in Fig. 2(b) (left axis). We simulate 128 individual spectra, and the averaged spectrum is shown as the black trace. The simulated SC is in good agreement with the experimental results. Slight discrepancies in the location of the dispersive waves between the simulation and experiment are attributed to deviations of the actual input power and dispersion from the simulated parameters. Experimentally, a small amount of the input light is coupled into higher-order modes, leading to a higher measured coupled power as compared to the simulation. We choose the pulse energy used in the simulation such that the simulated spectrum most closely reflects the experimentally generated SC. Additionally, the actual dispersion of the waveguide will vary slightly from the simulation dispersion due to waveguide fabrication tolerances.

The first-order, mutual-coherence function for the simulated SC is calculated based on [39]. As seen in Fig. 2(b) (right axis), the simulated SC has a coherence of unity over most of its bandwidth. This high-spectral coherence derives from the SC generation dynamics that accompanies pumping in the anomalous GVD regime with sufficiently short pulses [34]. Initially, the input pulse undergoes spectral broadening and temporal compression due to self-phase modulation (SPM). Symmetric spectral broadening due to SPM occurs over the first 6 mm of propagation in the waveguide, as seen in the spectral-evolution plot of Fig. 2(c). This is followed by the emission of short- and long-wavelength dispersive waves. For our high-energy pump pulses, a short-waveguide length is sufficient to generate broadband spectrum and helps preserve a coherent SC spectrum.

Next we demonstrate SCG using a 1-GHz repetition rate SESAM-modelocked diode-pumped Yb:CALGO laser [40]. This laser allows for a relatively easy coherence measurement due to the short delay in the path length (30 cm) between

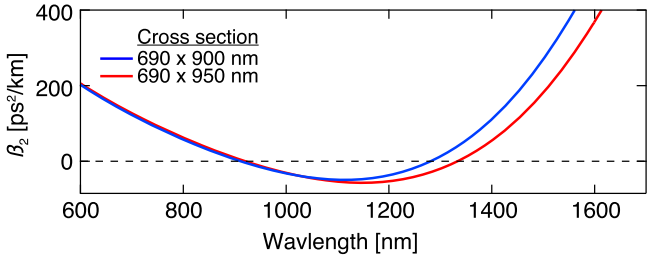

Fig. 1. Simulated GVD of Si_3N_4 waveguides with cross sections of 690 × 900 nm (blue) and 690 × 950 nm (red).

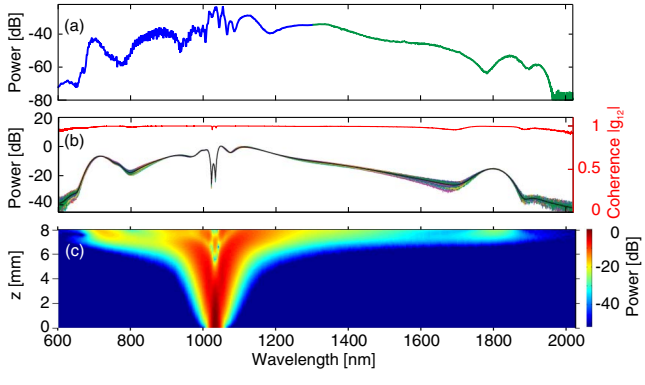

Fig. 2. (a) Experimental SCG spanning 1.7 octaves from an 8-mm-long Si_3N_4 waveguide with a 690 × 950 nm cross section. The blue and green regions indicate spectral components that are measured with the short- and long-wavelength OSAs, respectively. (b) Left axis: individually simulated SC spectra and the ensemble average (black). Right axis: spectral coherence for the simulated SC is near unity for the majority of the spectral bandwidth (red). (c) Spectral evolution of the simulated SC.

adjacent pulses. The laser pulses have a hyperbolic secant intensity profile and a center wavelength of 1055 nm. An optical Faraday isolator is used after the laser to protect against back reflections from the waveguide facet, and a grating pair is used to compensate for the GVD introduced by the isolator. Residual GVD and higher-order dispersion result in stretching of the laser pulses from 63-fs pulses before the isolator to 91-fs pulses after the isolator and grating pair. Back reflections from the waveguide can be suppressed in subsequent designs through use of an angled waveguide facet, eliminating the need for an isolator. The experimental setup is the same as described above. The Si_3N_4 waveguide is 7.5-mm-long with a 690 × 900 nm cross section. Figure 3(a) shows the SC generated with 236 pJ pulses incident on the waveguide with an 8-dB coupling loss. The measured SC is generated with 37 pJ of coupled pulse energy and exhibits similar spectral features to our previous results with a fiber laser (Fig. 2). The simulated SC of the 7.5-mm-long waveguide using 91-fs time-bandwidth-limited pump pulses and 24.5 pJ of coupled pulse energy is shown in Fig. 3(b) (left axis). The simulated spectrum corresponds closely with our experimental spectrum and displays a high degree of coherence over the entire spectral bandwidth [Fig. 3(b) (right axis)].

In order to experimentally characterize the coherence of the generated SC, we perform a spectral interference measurement [39,41] in which the output from the waveguide is sent to a free-space asymmetric Michelson interferometer. One arm of the interferometer is chosen to provide a delay corresponding to the pulse period. This allows for interference between adjacent pulses, creating interference fringes on the OSA when the SC generated by subsequent pulses are coherent. A single sweep of the OSA records the ensemble average of $>10^9$ interference events from which the first-order mutual coherence $[g_{12}^{(1)}(\lambda)]$ may be calculated according to [39]

$$|g_{12}^{(1)}(\lambda)| = \frac{V(\lambda)[I_1(\lambda) + I_2(\lambda)]}{2[I_1(\lambda)I_2(\lambda)]^{1/2}}, \quad \textbf{(1)}$$

where $I_1(\lambda)$ and $I_2(\lambda)$ are the measured spectral intensities from each arm of the interferometer, and $V(\lambda)$ denotes the fringe visibility, which is given by the maximum and minimum fringe intensity as $V(\lambda) = [I_{max}(\lambda) - I_{min}(\lambda)]/[I_{max}(\lambda) + I_{min}(\lambda)]$ [42].

For the coherence measurement, the temporal delay between interfering pulses is selected to give adequate resolution (fringe spacing) over the entire wavelength range. Light output from the interferometer is collimated into a fiber and sent to the OSA. We use a fiber that is single mode at 1550 nm for measurement of wavelengths longer than 1250 nm and a fiber that is single mode at 1060 nm for measurements performed below 1250 nm. This smaller core fiber ensures the spatial overlap between the interfering pulses at wavelengths longer than the cutoff wavelength. The spectral interference measurement is performed in 100-nm steps with optimization of the collimation and the alignment of the output for each wavelength region. The interference measurement is shown on the left axis of Fig. 4(a). As seen in Fig. 4(a) (left axis), interference fringes exist over the entire spectral range above the noise floor. The right axis of Fig. 4(a) gives the extracted visibility, which is near unity for the majority of the SC bandwidth. For measurements taken below the cutoff wavelength of the 1060 nm single-mode fiber (~890 nm) the multi-mode nature of the fiber leads to a sensitivity to the fiber collimator input coupling. This effect is seen in the reduction of the fringe extinction from 740 to 840 nm and in a decrease of the visibility, especially at the edges of the measurement range. Over the wavelength range from 840 to 1750 nm, the average visibility is 0.94. This high average visibility results from the high degree of phase coherence that exists between interfering pulses. As seen in Eq. (1), the visibility is equal to the first-order mutual coherence with the inclusion of a normalization factor that takes into account any differences in the intensities of the individual interferometer arms.

Importantly, we measure visibility near unity at spectral regions that are an octave apart, which enables f-$2f$ interferometry and detection of the f_{ceo} of the modelocked laser source. A magnified view of these spectral regions at 700 and 1400 nm is shown in the insets of Figs. 4(b) and 4(c). We measure an average visibility of 0.9 over the wavelength range from 675 to 725 nm and an average visibility of 0.99 over the wavelength range from 1350 to 1450 nm. For some wavelength regions we are limited by the signal-to-noise ratio of

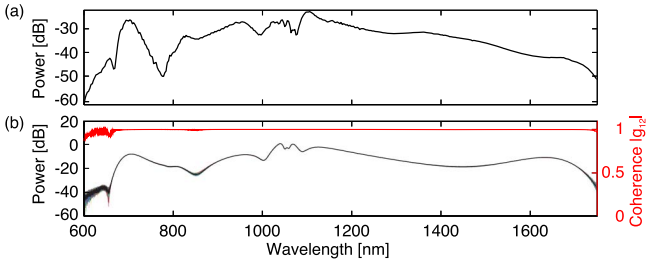

Fig. 3. (a) Experimental SCG for a 7.5-mm-long waveguide with 690 × 900 nm cross section and 37 pJ of coupled pulse energy. (b) Left axis: individually simulated SC spectra and ensemble average (black) for such a waveguide. Right axis: simulated coherence of the generated spectra is unity over the entire bandwidth.

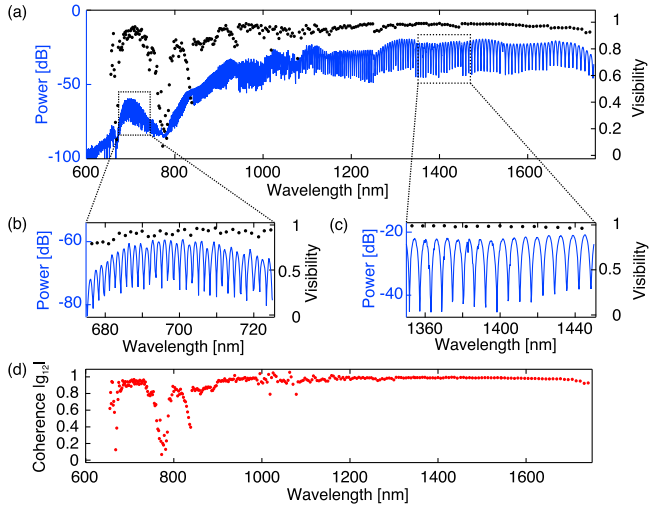

Fig. 4. (a) Left axis: experimental spectral interference measurement (blue) shows high extinction fringes over most of the SC bandwidth. Right axis: visibility (black) is close to unity over much of the wavelength range. (b),(c) Magnified view of the interference fringes and extracted visibility at (b) 700 nm and (c) 1400 nm. (d) Extracted coherence (red) is close to unity over much of the wavelength range.

the measured SC spectrum and thus could not extract the visibility. Lastly, we calculate the first-order mutual coherence pursuant to Eq. (1). The calculated coherence shown in Fig. 4(d) closely resembles the extracted visibility with slight differences due to the normalization factor. In the spectral region surrounding the pump wavelength we observe modulations in the measured intensity in the delay arm and reference arm of the interferometer, which distorts the coherence calculation.

In conclusion, we experimentally demonstrate SCG spanning over 1.4 octaves from a Si_3N_4 waveguide using a 53-MHz fiber laser and a 1-GHz Yb:CALGO laser. The simulated coherence for the SC generated from each laser is unity across the bandwidth of the spectrum. Additionally, we measure a coherent SC spectrum spanning from 670 to 1750 nm (measured at −30 dB relative to the peak of the spectrum) using the YB:CALGO laser. This represents a promising broadband coherent source for spectroscopy, frequency metrology, optical communications, and optical coherence tomography. Si_3N_4 provides a platform for coherent SC for diverse applications since it allows for tailoring the GVD and waveguide length to accommodate a variety of pump lasers with different pump wavelengths, pulse energies, and repetition rates. In addition, the demonstrated coherent octave-spanning bandwidth is ideal for the self-referenced detection of the f_{ceo} and illustrates the potential impact of a CMOS-compatible waveguide-based coherent SC source.

Funding. Air Force Office of Scientific Research (AFOSR) (FA9550-12-1-0377); Defense Advanced Research Projects Agency (DARPA) (QuASAR); National Science Foundation (NSF) (ECCS-1306035, ECS-0335765); Semiconductor Research Corporation (SRC); Swiss Innovation Promotion Agency (17137.1 PFMN-NM).

Acknowledgment. This work was performed in part at the Cornell NanoScale Facility, a member of the National Nanotechnology Infrastructure Network, which is supported by the NSF. We also acknowledge support of the technology and cleanroom facility FIRST of ETH Zurich for advanced micro- and nanotechnology. We thank Ron Synowicki from J. A. Woollam Co., Inc., for the characterization of the Si_3N_4 refractive index.

REFERENCES

1. I. Hartl, X. D. Li, C. Chudoba, R. K. Ghanta, T. H. Ko, J. G. Fujimoto, J. K. Ranka, and R. S. Windeler, Opt. Lett. **26**, 608 (2001).
2. H. Kano and H. Hamaguchi, Opt. Lett. **28**, 2360 (2003).
3. H. Kano and H. Hamaguchi, Appl. Phys. Lett. **86**, 121113 (2005).
4. L. F. Mollenauer, R. H. Stolen, J. P. Gordon, and W. J. Tomlinson, Opt. Lett. **8**, 289 (1983).
5. H. R. Telle, G. Steinmeyer, A. E. Dunlop, J. Stenger, D. H. Sutter, and U. Keller, Appl. Phys. B **69**, 327 (1999).
6. R. Holzwarth, T. Udem, T. W. Hänsch, J. C. Knight, W. J. Wadsworth, and P. St. J. Russell, Phys. Rev. Lett. **85**, 2264 (2000).
7. D. J. Jones, S. A. Diddams, J. K. Ranka, A. Stentz, R. S. Windeler, J. L. Hall, and S. T. Cundiff, Science **288**, 635 (2000).
8. S. A. Diddams, D. J. Jones, J. Ye, S. T. Cundiff, J. L. Hall, J. K. Ranka, R. S. Windeler, R. Holzwarth, T. Udem, and T. W. Hänsch, Phys. Rev. Lett. **84**, 5102 (2000).
9. I. Zeylikovich, V. Kartazaev, and R. R. Alfano, J. Opt. Soc. Am. B **22**, 1453 (2005).
10. S. Schiller, Opt. Lett. **27**, 766 (2002).
11. I. Coddington, W. C. Swann, and N. R. Newbury, Phys. Rev. Lett. **100**, 013902 (2008).
12. F. Leo, S.-P. Gorza, J. Safioui, P. Kockaert, S. Coen, U. Dave, B. Kuyken, and G. Roelkens, Opt. Lett. **39**, 3623 (2014).
13. B. Kuyken, X. Liu, and R. M. Osgood, Jr., R. Baets, G. Roelkens, and W. M. J. Green, Opt. Express **19**, 20172 (2011).
14. F. Leo, S.-P. Gorza, S. Coen, B. Kuyken, and G. Roelkens, Opt. Lett. **40**, 123 (2015).
15. B. Kuyken, T. Ideguchi, S. Holzner, M. Yan, T. W. Hänsch, J. V. Campenhout, P. Verheyen, S. Coen, F. Leo, R. Baets, G. Roelkens, and N. Picqué, Nat. Commun. **6**, 6310 (2015).
16. R. K. W. Lau, M. R. E. Lamont, A. Griffith, Y. Okawachi, M. Lipson, and A. L. Gaeta, Opt. Lett. **39**, 4518 (2014).
17. F. Leo, J. Safioui, B. Kuyken, G. Roelkens, and S.-P. Gorza, Opt. Express **22**, 28997 (2014).
18. D. Y. Oh, D. Sell, H. Lee, K. Y. Yang, S. A. Diddams, and K. J. Vahala, Opt. Lett. **39**, 1046 (2014).
19. D. Duchesne, M. Peccianti, M. R. E. Lamont, M. Ferrera, L. Razzari, F. Lëgarë, R. Morandotti, S. Chu, B. E. Little, and D. J. Moss, Opt. Express **18**, 923 (2010).
20. R. Halir, Y. Okawachi, J. S. Levy, M. A. Foster, M. Lipson, and A. L. Gaeta, Opt. Lett. **37**, 1685 (2012).
21. J. M. Chavez Boggio, T. Fremberg, D. Bodenmüller, R. Eisermann, R. Haynes, L. Zimmermann, and M. Roth, *Advanced Photonics* (Optical Society of America, 2014), paper JTu3A.54.
22. J. M. Chavez Boggio, D. Bodenmüller, T. Fremberg, R. Haynes, M. M. Roth, R. Eisermann, M. Lisker, L. Zimmermann, and M. Böhm, J. Opt. Soc. Am. B **31**, 2846 (2014).
23. H. Zhao, B. Kuyken, S. Clemmen, F. Leo, A. Subramanian, A. Dhakal, P. Helin, S. Severi, E. Brainis, G. Roelkens, and R. Baets, Opt. Lett. **40**, 2177 (2015).
24. A. S. Mayer, A. Klenner, A. R. Johnson, K. Luke, M. R. E. Lamont, Y. Okawachi, M. Lipson, A. L. Gaeta, and U. Keller, Opt. Express **23**, 15440 (2015).
25. J. P. Epping, T. Hellwig, M. Hoekman, R. Mateman, A. Leinse, R. G. Heideman, A. van Rees, P. J. M. van der Slot, C. J. Lee, C. Fallnich, and K.-J. Boller, Opt. Express **23**, 19596 (2015).
26. R. Salem, Y. Okawachi, M. Yu, M. R. E. Lamont, K. Luke, P. Fendel, M. Lipson, and A. L. Gaeta, *Conference on Lasers and Electro-Optics* (Optical Society of America, 2015), paper STu1I.7.
27. M. R. E. Lamont, B. Luther-Davies, D.-Y. Choi, S. Madden, and B. J. Eggleton, Opt. Express **16**, 14938 (2008).
28. S. Xie, F. Tani, J. C. Travers, P. Uebel, C. Caillaud, J. Troles, M. A. Schmidt, and P. St. J. Russell, Opt. Lett. **39**, 5216 (2014).
29. Y. Yu, X. Gai, P. Ma, D.-Y. Choi, Z. Yang, R. Wang, S. Debbarma, S. J. Madden, and B. Luther-Davies, Laser Photon. Rev. **8**, 792 (2014).
30. N. D. Psaila, R. R. Thomson, H. T. Bookey, S. Shen, N. Chiodo, R. Osellame, G. Cerullo, A. Jha, and A. K. Kar, Opt. Express **15**, 15776 (2007).
31. C. R. Phillips, C. Langrock, J. S. Pelc, M. M. Fejer, J. Jiang, M. E. Fermann, and I. Hartl, Opt. Express **36**, 3912 (2011).
32. D. J. Moss, R. Morandotti, A. L. Gaeta, and M. Lipson, Nat. Photonics **7**, 597 (2013).
33. K. Narayanan and S. F. Preble, Opt. Express **18**, 8998 (2010).
34. J. M. Dudley, G. Genty, and S. Coen, Rev. Mod. Phys. **78**, 1135 (2006).
35. M. Erkintalo, Y. Q. Xu, S. G. Murdoch, J. M. Dudley, and G. Genty, Phys. Rev. Lett. **109**, 223904 (2012).
36. H. Lim, F. Ö. Ilday, and F. W. Wise, Opt. Lett. **28**, 660 (2003).
37. K. Luke, A. Dutt, C. B. Poitras, and M. Lipson, Opt. Express **21**, 22829 (2013).
38. A. Ruehl, M. J. Martin, K. C. Cossel, L. Chen, H. McKay, B. Thomas, C. Benko, L. Dong, J. M. Dudley, M. E. Fermann, I. Hartl, and J. Ye, Phys. Rev. **84**, 011806 (2011).
39. X. Gu, M. Kimmel, A. P. Shreenath, R. Trebino, J. M. Dudley, S. Coen, and R. S. Windeler, Opt. Express **11**, 2697 (2003).
40. A. Klenner, S. Schilt, T. Südmeyer, and U. Keller, Opt. Express **22**, 31008 (2014).
41. F. Lu and W. H. Knox, Opt. Express **12**, 347 (2004).
42. J. W. Nicholson and M. F. Yan, Opt. Express **12**, 679 (2004).